HHS Public Access

Author manuscript

Biomaterials. Author manuscript; available in PMC 2017 January 01.

Published in final edited form as:

Biomaterials. 2016 January ; 76: 52–65. doi:10.1016/j.biomaterials.2015.10.046.

Targeted drug delivery to circulating tumor cells via platelet membrane-functionalized particles

Jiahe Li[1,2,*], **Yiwei Ai**[3], **Lihua Wang**[3], **Pengcheng Bu**[3], **Charles C. Sharkey**[1], **Qianhui Wu**[1], **Brittany Wun**[1], **Sweta Roy**[1], **Xiling Shen**[3], and **Michael R. King**[1,*]

[1]Department of Biomedical Engineering, Cornell University, Ithaca, New York, USA, 14853

[3]Department of Biomedical Engineering, Duke University, Durham, North Carolina, USA, 27708

Abstract

Circulating tumor cells (CTCs) are responsible for metastases in distant organs via hematogenous dissemination. Fundamental studies in the past decade have suggested that neutralization of CTCs in circulation could represent an effective strategy to prevent metastasis. Current paradigms of targeted drug delivery into a solid tumor largely fall into two main categories: unique cancer markers (e.g. overexpression of surface receptors) and tumor-specific microenvironment (e.g. low pH, hypoxia, etc.). While relying on a surface receptor to target CTCs can be greatly challenged by cancer heterogeneity, targeting of tumor microenvironments has the advantage of recognizing a broader spectrum of cancer cells regardless of genetic differences or tumor types. The blood circulation, however, where CTCs transit through, lacks the same tumor microenvironment as that found in a solid tumor. In this study, a unique “microenvironment” was confirmed upon introduction of cancer cells of different types into circulation where activated platelets and fibrin were physically associated with blood-borne cancer cells. Inspired by this observation, synthetic silica particles were functionalized with activated platelet membrane along with surface conjugation of tumor-specific apoptosis-inducing ligand cytokine, TRAIL. Biomimetic synthetic particles incorporated into CTC-associated micro-thrombi in lung vasculature and dramatically decreased lung metastases in a mouse breast cancer metastasis model. Our results demonstrate a “Trojan Horse” strategy of neutralizing CTCs to attenuate metastasis.

Keywords

CTC; platelets; silica microparticles; metastasis

[*]Contact information: Jiahe Li, Koch Institute for Integrative Cancer Research, 77 Massachusetts Ave., Cambridge, MA 02139. Phone: 617-523-6443; jiaheli@mit.edu. Michael R. King, 205 Weill Hall, Ithaca, NY 14853. Phone: 607-255-9803; mike.king@cornell.edu.

[2]Current address: Department of Chemical Engineering, Massachusetts Institute of Technology, Cambridge, Massachusetts, USA, 02139

Conflict of interest: No conflicts of interest declared

Introduction

Metastasis contributes to more than 90% of cancer-associated mortality. It occurs after primary tumors shed circulating tumor cells (CTCs) via hematogenous dissemination to distant organs [1, 2]. Despite advancements in the fundamental biology and diagnosis of CTCs, effective neutralization of CTCs for the prevention of metastasis remains clinically challenging. Existing nano-medicines for cancer treatment aim to target solid tumors (primary and metastatic tumors). The underlying principle is largely based on the enhanced permeability and retention (EPR) effect in which nanoparticles and macromolecules drain into tumor-associated leaky vasculatures and are retained in tumors due to inefficient lymphatic drainage [3, 4]. Although it has been proven to be a key paradigm for existing nano-medicines, the EPR effect, however, may not be readily translated to the targeting of CTCs in circulation. The physical environment surrounding CTCs is different from that of solid tumors [5]. In solid tumors, high interstitial fluid pressure represents a major barrier to the delivery of nano-medicine caused by enhanced stiffness of extracellular matrices and leaky tumor-associated vasculature [6, 7]. In contrast, CTCs are exposed to a broad range of fluid shear stresses when transiting in different vascular compartments (arteries, veins and capillaries). The mobile nature of CTCs and varied fluid shear stresses may have a major impact on the effectiveness of nano-medicines against CTCs.

During their transit in the blood circulation, CTCs are subjected to destruction by natural killer cells, neutrophils, macrophages and cytotoxic T cells [8–11]. Nevertheless, CTCs can locally induce thrombosis, including platelet activation and fibrin deposition, to form a protective cloak, which in turn protects CTCs from an immune attack [8, 12, 13]. These two dueling forces counteract each other to determine the survival of CTCs in the circulation and eventually the likelihood of developing distant metastases. Current immunotherapies that boost the cytotoxicity of immune cells (natural killer cells and cytotoxic T cells) via systemic injection of cytokines such as IL-2 and IFN-α may tip the balance in favor of CTC neutralization. Unfortunately, this strategy under certain circumstances can elicit a life-threatening cytokine storm caused by over-reactivity of the immune system [14, 15]. Alternatively, anti-thrombosis drugs have been demonstrated as an effective means of reducing metastasis in mouse cancer models. These drugs, however, can in principle interfere with the normal hemostatic function of thrombosis, which eventually leads to bleeding disorders [16, 17]. In general, these two different approaches can potentially cause severe side effects by disrupting homeostasis of the immune and hemostatic systems.

To leverage the strength of the immune boosting approach and circumvent the side effects associated with anti-thrombosis therapies, a Trojan horse strategy was developed in this work. Inspired by the adhesion of activated platelets to CTC-associated micro-thrombi, biocompatible silica (Si) particles were functionalized with membrane-derived vesicles from activated platelets. This biomimetic coating allows for targeting of synthetic particles to CTCs. Additionally, the major tumor-killing cytokine, Tumor necrosis factor – related apoptosis inducing ligand (TRAIL) was conjugated to the platelet membrane-coated Si particles. TRAIL is highly expressed on the surface of cancer-killing natural killer cells, activated neutrophils and cytotoxic T cells [18, 19]. Such a system takes advantage of CTC adhesion to activated platelets and the tumoricidal activity of immune cells to produce a

targeted therapeutic effect. Moreover, synthetic particles camouflaged with platelet membrane were incorporated into CTC-induced thrombosis in the vasculature to deliver cancer-killing drugs within CTC thrombi at a high local concentration.

Methods and Materials

Cell lines and mice

Human breast cancer cell line MDA-MB-231, prostate cancer cell line PC3, and umbilical vein endothelial cells (HUVECs) were obtained from American Type Culture Collection (ATCC, Rockville, MD, USA). MDA-MB-231 cells were cultured in DMEM (Invitrogen, Grand Island, NY, USA) with 10% FBS. PC3 cells were maintained in RPMI (Invitrogen) with 10% FBS and HUVECs were expanded in vascular cell basal medium (ATCC) using the endothelial cell growth kit-BBE (ATCC). HUVECs were used up to passage number 6. Six to eight week old female NOD SCID gamma mice were purchased from Jackson Laboratory (Bar Harbor, ME, USA). Mice were housed in a SPF barrier animal facility at Cornell University.

Chemicals and antibodies

His-tagged TRAIL for *in vivo* work was produced and purified as previously described [20]. The following chemicals or kits were used for assaying cell proliferation and apoptosis: MTT (AMRESCO, Solon, OH, USA) and TACS® Annexin V-FITC Kit (Gaithersburg, MD, USA). Reagents for SEM and TEM were obtained from Electron Microscopy Sciences (Hatfield, PA, USA): glutaraldehyde, osmium tetroxide and uranyl acetate. APC-conjugated antibodies specific for the extracellular domains of human CD41, CD42b, CD47, CD61 and CD62P in flow cytometry and fluorescence microscopy studies were purchased from Biolegend (San Diego, CA, USA). Primary CD41 antibodies for the extracellular domain (M-148) and cytoplasmic domain (B-9) detection and human CD47 blocking antibody (B6H12) were from Santa Cruz Biotech (Dallas, TX, USA).

Synthesis of silica particles

Monodisperse silica (Si) particles with a diameter of 2–3 μm were synthesized using tetraethyl orthosilicate (TEOS), 29% ammonia and 100% ethanol via the Stöber method. To produce a positively charged surface, Si particles were suspended in ethanol containing 1 mg/ml 3-aminopropyl triethoxysilane (APTES) and stirred overnight. To prepare FITC-labeled Si particles, FITC was first reacted with APTES in the presence of ethanol and ammonia. Afterwards, TEOS was added to FITC dye solution and stirred overnight to form FITC-labeled Si particles. All synthesized Si particles were washed three times with 100% ethanol followed by three times with TBS to remove free substrate. Particles were characterized with dynamic light scattering using a Zetasizer (Malvern Instruments, Malvern, Worcestershire, UK) and LEO 1550 FE-SEM (Zeiss, Atlanta, GA, USA) prior to PMDV coating.

Preparation and functionalization of PMDVs to Si particles

Platelets were pelleted from platelet-rich plasma (PRP) through differential centrifugation of whole blood. Following three washes to remove plasma proteins, the isolated platelets were

fragmented by seven freeze-thaw cycles and sonication to release platelet membrane-derived vesicles. Then, ultracentrifugation with a discontinuous sucrose gradient (5%, 40%, 55%) was performed to separate membrane vesicles from free proteins, intact platelets, and high-density granules. Previous studies have examined the electrostatically mediated deposition and fusion of negatively charged liposomes on cationic particle supports [27, 28]. In light of the negative surface charge of PMDVs, Si particles with diameters close to platelet size were functionalized with (3-Aminopropyl) triethoxysilane (APTES) to produce a positive charge on the surface. Subsequently, PMDVs were immobilized on the positively charged particle surface by incubating 100 μg PMDVs with 10 million particles. After removing free vesicles from the mixture, the coated particles were characterized by dynamic light scattering and electron microscopy.

Membrane protein profiling by LC-MS

PMDV-coated particles were washed three times with TBS. On-bead tryptic proteolysis protocol was performed. Briefly, proteins were reduced by adding 5 mM DTT (45 min, 56°C), and free cysteines were alky lated with iodoacetamide (15 mM, 25°C, 1 hr in the dark). A sample of 0.2 μg porcine sequencing grade trypsin (Promega, Mannheim, Germany) were added and the samples were incubated overnight at 37°C. After digestion, the r eaction was stopped with 10 μL of 10% formic acid (FA). The resulting precipitate and particles were removed by centrifugation (13,000 x g, 15 min, 4°C). Supernata nt was transferred for LC-MS analysis. Capillary liquid chromatography of tryptic peptides was performed with UltiMate® 3000 RSLCnano LC system (Thermo, Chelmsford, MA, USA). Mass spectrometry analysis of tryptic peptides was performed using Orbitrap Elite (Thermo).

Flow cytometry and fluorescence microscopy

PMDV-coated and uncoated Si particles were suspended at a concentration of 1 million per 100 μL blocking buffer PBS/1% BSA. APC-conjugated primary antibodies were added in the blocking buffer and incubated for 30 min at room temperature. Following three washes with 1 mL of PBS, fluorescence measurements were collected using a Guava flow cytometer (EMD, Billerica, MA, USA). Data were analyzed using the Flow Express software (De Novo Software, Los Angeles, CA, USA). For fluorescence microscopy detection, stained particles were first immobilized on poly-lysine coated glass slides. Images were acquired in an upright Olympus BX-50 microscope.

SEM and TEM

PMDV-coated Si particles were fixed in 2.5% glutaraldehyde and 1% osmium tetroxide. Samples were serially dehydrated in 25%, 50%, 75%, 95% and 100% ethanol. Samples used for SEM were subjected to critical point drying followed by carbon sputter coating. Particles were imaged using a LEO 1550 FE-SEM at an accelerating voltage of 3kv with a 3mm working distance. For TEM, after ethanol dehydration, samples were immobilized on carbon-coated copper grids and counterstained briefly with 2% uranyl acetate. Images were taken by a FEI T12 Spirit TEM STEM (Tecnai, Hillsboro, OR, USA) at 120kv.

Preparation of fibrin-functionalized microtubes for in vitro thrombosis model

50 cm-long microrenathane microtubes with an inner diameter of 300 μm (Braintree Scientific, Braintree, MA, USA) were first washed with 1× PBS and then coated with 1 mg/ml human fibrinogen for 1 hr at RT. In negative control microtubes, 1 mg/ml human albumin was used instead. Afterwards, $CaCl_2$ (20 mM) and human α-thrombin (1 U/ml, Enzyme Research Laboratories, IN) in TBS were infused into microtubes and incubated for 1 hr at RT. All microtubes were blocked with 1% BSA to prevent nonspecific adhesion. Functionalized microtubes were then secured to the stage of an Olympus IX81 motorized inverted microscope (Olympus America, Melville, NY). After washing microtubes with TBS, PMDV-coated Si particles and uncoated particles at a concentration of 1×10^6 per ml in TBS plus Ca^{2+}, EDTA or Ca^{2+} plus 1mg/ml fibrinogen were perfused at 4 dyn/cm^2 using a syringe pump (IITC Life Sciences, Woodland Hills, CA, USA). A CCD camera (Hitachi, Tokyo, Japan) and DVD recorder (Sony Electronics, Tokyo, Japan) were used to record experiments for offline analysis.

Conjugation of TRAIL to PMDV-coated Si particles

Samples of 1 mg/ml recombinant human TRAIL or PMDV-coated Si particles with an equivalent protein concentration of 1 mg/ml were incubated with 10-fold molar excess of sulfo-NHS-biotin (Thermo) for 30 min at room temperature. Excess linkers were removed from TRAIL using a desalting column (Thermo) or from Si particles by centrifugation (1000g, 3 min). Streptavidin (Thermo) was used to conjugate TRAIL to PMDV-coated Si particles at a 1:1 molar ratio of streptavidin to TRAIL. Concentrations of TRAIL were adjusted based on the desired TRAIL density (0.2, 0.5 and 1 μg per mg of particles) on PMDV-coated Si particles. TRAIL-conjugated particles were washed with PBS three times prior to in vitro and in vivo assays.

Cell proliferation assay

Cell proliferation was assayed by measuring mitochondrial dehydrogenase activity using MTT as the substrate. At experimental end points, cells were incubated with MTT at a concentration of 0.5 mg/mL, at 37°C for 3 hr. The purple MTT product was solubilized with DMSO and measured at 570nm using a BioTek plate reader (Winooski, VT, USA).

Experimental lung metastasis assays

All mice were handled according to the Guide for the Care and Use of Laboratory Animals in compliance with US- and UK-based guidelines. All experimental procedures and protocols were approved by the Institutional Animal Care and Use Committee of Cornell University (Protocol No. 2011-0051). In the study of cancer cell-induced thrombosis in blood circulation, cells were labeled with Calcein-AM for the imaging of colocalization of cancer cells with platelets. CellTracker™ Red CMTPX (Invitrogen) was used to label cancer cells to visualize colocalization of the cells with FITC-labeled particles. Fluorescent cells were injected into 6–8 week-old C57BL/6 or Nod SCID gamma (NSG) mice via tail vein injection at 1×10^6 cells per 0.1ml in PBS. To visualize cancer cell-platelet interactions, mice were euthanized after 30 min for sample embedding. For colocalization of cancer cells and Si particles mice received 5×10^7 FITC-labeled PMDV-coated Si particles or uncoated

particles through retro-orbital injection 30 minutes after the cell injection. Mice were then euthanized 30 minutes after receiving the injection of particles. The lungs were removed, embedded in OCT, and snap frozen in liquid nitrogen. Embedded samples were sectioned to a thickness of 8 μm by cryostat (Tissue-Tek®, Torrance, CA, USA) and mounted on glass slides. Platelets were stained by anti-CD41 (Biolegend).

In vivo therapeutic treatment and bioluminescence imaging

A sample of 1×10^5 MDA-MB-231 cells expressing firefly luciferase were injected into NSG mice via tail vein injection. TRAIL-conjugated PMDV-Si particles or control groups (1 μg TRAIL per mg of silica) were injected via retro-orbital injection at 30, 90 and 120 min after the injection of cancer cells at a particle-to-cell ratio of 50 : 1. Bioluminescent imaging was performed with a CCD camera mounted in a light-tight specimen box (Xenogen, Waltham, MA, USA) at weeks 2 and 4 after the injection of cancer cells. Imaging and quantification of signals were controlled by the acquisition and analysis software Living Image® (Xenogen). Anesthetized mice were placed in the IVIS™ Imaging System and imaged from ventral views approximately 10–15 min after intraperitoneal injection of D-luciferin at 150 mg/kg body weight. Metastatic burden was quantified by measuring bioluminescence intensity normalized to imaging area and exposure time.

Tail bleeding assay

Tail bleeding time was determined by removing 3 mm of the distal mouse tail and immediately immersing the tail in 37°C PBS. A compl ete cessation of bleeding was defined as the end point of bleeding time.

Statistical analysis

All statistical analyses were performed using GraphPad Prism 5.0a for Mac OS X (San Diego, CA, USA). A one-way ANOVA followed by Tukey post test was used to compare statistical significance in the characterization of *in vitro* cell proliferation and *in vivo* experiments.

Results

Observation of cancer cell/fibrin/platelet thrombi in experimental lung metastasis model

Previous studies have provided *in vitro* evidence that multiple types of human cancer cells could activate thrombosis involving platelet adhesion and fibrin deposition. In experimental mouse metastasis models, treatments with an antibody or a chemical to interfere with coagulation led to reduced frequency of metastases [16, 17, 21]. Nevertheless, it remains unclear how cancer cells and thrombosis spatially and physically interact in the vasculature. To address this question, an experimental lung metastasis model was chosen for two reasons: 1. The lungs are the most frequently metastatic organs in multiple types of cancer including breast, prostate, melanoma and colon cancers [22–25]. 2. The highly vascularized structure of the lungs allows for facile visualization of CTC-fibrin-platelet emboli in circulation [26]. Fluorescently labeled human breast cancer cells MDA-MB-231 and colon cancer cells COLO 205 were inoculated into the blood circulation of separate NSG immunocompromised mice. After 30 min, the lungs were collected, immediately fixed with

formaldehyde, and snap frozen by liquid nitrogen for tissue sectioning. The combined chemical and physical fixation procedure provided a “snapshot” of interplay between cancer cells and blood components. Subsequent immunofluorescence staining for fibrin and activated platelets demonstrated colocalization of cancer cells, fibrin and platelets in lung vasculatures despite their systemic nature (Figure 1a and b). To rule out the species difference, syngeneic mouse metastasis models were tested by injecting C57BL/6-derived colon cancer cells MC38 and melanoma cancer cells B16-F10 into C57BL/6 mice via the tail vein, respectively. The same trend of colocalization patterns were observed (Figure 1c and d). *In vitro* expanded cell lines may have lost their host-derived signatures after extended passage and therefore may “stick” to platelets, as platelets are excellent opsonins. To exclude such possibility, B16-F10 cells were subcutaneously (s.c.) implanted in C57BL/6 mice to generate an orthotopic melanoma mouse model. After palpable tumors were visible, they were subjected to collagenase D dissociation to single cells and rejected into C57BL/6 mice intravenously. It was found that those cells were still able to colocalize with platelets and fibrin inside mouse lung vasculature (Supplemental figure 1). The experimental metastasis models demonstrated that cancer cells physically interacted with fibrin and activated platelets in circulation. This suggests that synthetic particles functionalized with activated platelet-derived membrane components may exploit this interaction for the targeting of CTCs.

Functionalization of Si particles with platelet membrane

The preparation of platelet membrane-coated Si particles involves two major steps: extraction of platelet membrane-derived vesicles (PMDVs) from activated platelets, and vesicle-particle fusion (Figure 2a). Two distinct lipid layers were formed at the interfaces of the 5%–40% and 40%–55% sucrose layers after ultracentrifugation. To identify which fraction contained PMDVs, a dot blot assay was performed to stain two platelet integral membrane proteins (CD41a and CD47) in each fraction (0.5 mL) of the sucrose gradient. It was found that the majority of membrane vesicles existed at the interface between 5% and 40% (Figure 2b). The z-average diameter of vesicles was 106 ± 32 nm with a zeta potential of −10 mV, close to the surface charge of intact platelets (Table 1). The morphology of vesicles was characterized and displayed hollow structure under TEM (Figure 2c).

After coating Si particles with PMDVs, the coated particles were found to be close to uncoated particles in size. In contrast, the surface zeta potential changed from +25.5 ± 4.6 mV (APTES-particles) to −10.1 ± 1.9 mV (coated particles), close to that of PMDVs and platelets (Table 1). Furthermore, SEM and TEM imaging revealed a coating of the platelet membrane on the surface of Si particles, in comparison to uncoated ones. Fusion between adjacent proteo-lipid patches and lipid vesicles likely resulted in complete coverage of the particle surface (Figure 2c).

Detection of platelet membrane proteins on coated particles

Integral membrane proteins are essential for adhesion of activated platelets to CTC-induced fibrin clots. To examine the presence and stability of proteins on functionalized Si particles, membrane proteins were stripped from PMDV-coated Si particles after incubation in TBS at 37 °C for 1 2, 24, and 48 hr and were resolved by SDS-PAGE. Commassie blue staining of

the protein gel confirmed that the compositions of membrane proteins present on Si particles throughout different incubation times were largely identical to the compositions of platelet membranes (Figure 3a). The stability of PMDV attachment to the Si particle surface was examined by incubating coated particles in fetal bovine serum at 37 °C for 12, 24, and 48 hr. An equivalent number of p articles was subjected to western blotting. A platelet membrane-associated protein, CD41, was used as a “surrogate” marker to estimate the quantity of PMDVs. It was found that PMDVs remained on the surface of Si particles for at least 24 hr in serum despite that certain protein losses were detected at the 48 hr time point (Supplemental figure 2).

To profile membrane proteins on PMDV-coated Si particles, an on-bead trypsin digestion was performed, followed by liquid chromatography-mass spectrometry (LC-MS). The top membrane proteins were identified based on their relative abundance (Table 2). To further validate protein identity from LC-MS, key proteins involved in platelet adhesion (CD41, CD42b and CD61) and anti-phagocytosis (CD47) were detected on PMDV-coated Si particles by antibodies recognizing the extracellular domain of each membrane protein (Figure 3b and c). In addition to proteins, glycans (sialic acid and N-acetylglucosaminyl residues) are key post-translational modifications for membrane protein-mediated cell-cell or cell-fibrin adhesion. The presence of sialic acid and *N*-acetylglucosaminyl residues on PMDV-coated Si particles was identified by staining with Alexa Fluor® 488-conjugated wheat germ agglutinin (WGA) and analyzed via flow cytometry and immunostaining (Figure 3d and e). To investigate the orientation of native proteins on PMDV-coated Si particles, CD41, a single-pass type I membrane protein composed of a N terminal extracellular domain, a transmembrane region and a C terminal cytoplasmic domain, was selected due to its simple structure as well as abundant expression on the platelet membrane. Two antibodies recognizing extracellular and cytoplasmic domains of CD41 were used in flow cytometry. It was found that the majority of CD41 was present in an extracellular-outward orientation with a 4:1 ratio of extracellular-to-cytoplasmic domains on the outer surface of PDMV-coated Si particles (Supplemental figure 3).

Platelet membrane coating reduces phagocytic uptake of particles

Phagocyte-mediated phagocytosis of synthetic particles may present a major barrier to efficient delivery to CTCs in the circulatory system. The ability of platelet membrane camouflage to reduce particle phagocytosis was studied using a well-characterized phagocytic cell line, THP-1. First, THP-1 cells were differentiated with 100 ng/ml phorbol 12-myristate 13-acetate (PMA) for 48 hr. In preparation for the phagocytosis assay, FITC-labeled uncoated and PMDV-coated Si particles were incubated with human plasma to allow for opsonization by serum proteins at 37°C for 30 min. Afterwards, d ifferentiated cells were incubated with an equivalent number of two different Si particles respectively at 37°C for 2 hr. After enzymatic removal of surface-b ound particles by trypsin, THP-1 cells with internalized particles were quantified using flow cytometry. It was found that the PMDV coating significantly reduced particle phagocytosis in comparison to uncoated particles (Figure 4a and b). Additionally, fluorescent microscopy confirmed that more uncoated Si particles were internalized into the cytoplasm of THP-1 cells (Figure 4c). Notably, after opsonization, uncoated and coated particles exhibited a surface zeta potential of −9.2 ± 1.1

mV and −10.8 ± 1.7 mV, respectively, which rules out the influence of charge difference on particle adhesion and internalization in the THP-1 phagocytosis assay (Supplemental table 1). To investigate the mechanism of reduced phagocytosis in PMDV-coated Si particles, absorption of IgG to uncoated and coated Si particles was compared, since the extent of antibody (especially IgG) opsonization to exogenous materials has been found to correlate with the level of phagocyte-mediated phagocytosis [27]. Using FITC-labeled anti-human IgG antibody, it was shown that uncoated Si particles absorbed more IgG than PMDV-coated ones (Figure 4d). The differential opsonization with IgG likely explained the reduced phagocytosis for coated Si particles. In addition to differential IgG opsonization, CD47 was also found to be essential for reduced phagocytosis in PMDV-coated Si particles. Treating coated particles with CD47 blocking antibody was able to increase phagocytosis of coated particles in THP-1 cells (Figure 4e).

Adhesion of PMDV-coated Si particles to fibrin under flow

Upon release of CTCs into circulation, tissue factor on the cells convert prothrombin (inactive) to thrombin (active) in plasma, which in turn induces platelet activation, fibrin deposition and recruitment of activated platelets to fibrins [12]. To investigate the capability of PMDV-coated Si particles to target fibrin in a microvessel under flow conditions, a previous protocol for preparing fibrin-immobilized polystyrene beads was adopted to prepare an *in vitro* thrombosis model in microtubes [28]. Briefly, after immobilizing 1mg/ml fibrinogen on the microtube surface, thrombin was added to form fibrin. Particles were perfused at a defined shear stress controlled by a syringe pump and the adhesion events were recorded with a CCD camera mounted on a microscope (Figure 5a). To compare the adhesion dynamics of PDMV-coated Si particles to that of activated platelets, an equal density of particles or cells suspended in tris-buffered saline (TBS) plus Ca^{2+} were perfused through fibrin-functionalized microtubes under physiological wall shear stresses in veins (4 and 8 dyn/cm^2). It was found that adhesion events of both particles and platelets increased over time but decreased with increasing shear stress. In addition, PMDV-coated Si particles adhered slightly less efficiently to fibrin surfaces than activated platelets (Figure 5b).

To confirm that the binding of PMDV-coated Si particles was fibrin-dependent, it was verified that the albumin-coated surface failed to induce particle adhesion in microtubes. Moreover, replacement of Ca^{2+} with EDTA abolished the adhesion of particles to the fibrin surface (Figure 5c). This observation was consistent with the fact that the adhesion of activated platelets to fibrin is Ca^{2+}-dependent.

To simulate physiologically relevant conditions, PMDV-coated Si particles were suspended in TBS containing 2 mg/ml soluble fibrinogen which, in principle, binds to the same $\alpha_{II\beta}/\beta_3$ (CD41/CD61) integrins on activated platelets as fibrin. Interestingly, despite the presence of competitive fibrinogen in suspension, PMDV-coated Si particles under flow conditions were able to bind to immobilized fibrin with a comparable efficiency as in TBS Ca^{2+} (Figure 5d). Furthermore, a more physiologically relevant condition was tested by suspending PMDV-coated Si particles in platelet-poor plasma (PPP). It was found that this more complex environment did not significantly interfere with the active adhesion of particles to the fibrin-coated surface under flow (Figure 5d and e). It is possible that activated $\alpha_{II\beta}/\beta_3$ (CD41/

CD61) integrins on PMDV-coated Si particles tend to bind to surface-bound fibrin more efficiently than the free form of fibrinogen. Nevertheless, such observations mirror the adhesion of activated platelets to thrombi in the presence of abundant fibrinogens in plasma. Moreover, the potential of PMDV-coated Si particles to adhere to fibrin in a complex body fluid environment suggests that they could be utilized to target thrombi induced by cancer cells or certain cardiovascular disease states.

TRAIL-conjugated PMDV-Si particles induce apoptosis in cancer cells

TRAIL is highly expressed on the surface of natural killer cells, activated neutrophils, and cytotoxic T cells and is largely responsible for the anti-tumor effect of immune cells. In contrast, TRAIL expression was not detectable on the surface of human or mouse platelets (Supplemental Figure 4). We next explored whether conjugation of TRAIL to the surface of PMDV-coated Si particles could induce apoptosis in cancer cells. TRAIL was conjugated to coated Si particles via a NHS-biotin/streptavidin linkage and the maximum loading yield without particle aggregation was found to be ~1 μg of TRAIL per mg of Si particles (~10^7 Si particles) by Bradford and ELISA assays. To confirm the stability of the TRAIL linkage to PMDV-coated Si particles, TRAIL-conjugated PMDV-Si particles were incubated with FBS at 37 °C for 12, 24, and 48 hr. It was found that despite the reduction of conjugated TRAIL by the 48 hr time point, no significant loss of TRAIL was detected within the initial 24 hrs (Supplemental figure 5). Next, TRAIL conjugation density was varied at 0.2, 0.5 and 1 μg per mg of particles for *in vitro* incubation with MDA-MB-231 (breast cancer) and PC3 (prostate cancer) cells. In addition, cancer cells were incubated with TRAIL-conjugated particles at different particle-to-cell ratios. It was found that the reduction of cell viability by TRAIL-conjugated Si particles was dependent on both TRAIL coating density and particle-to-cell ratio (Figure 6a). In contrast, when the HUVEC endothelial cells, which serve as a normal cell control, were incubated with PMDV-coated particles with 1 μg TRAIL per mg of silica at different particle-to-cell ratios, no growth inhibition was detected relative to PMDV-coated particles without TRAIL (Figure 6b). Furthermore, to examine whether the NHS-biotin/streptavidin crosslinking would compromise TRAIL activity, PMDV-coated particles with 1 μg TRAIL per mg of silica were incubated with cancer cells at different particle-to-cell ratios and compared to an equivalent amount of soluble TRAIL for each ratio. It was found that the surface conjugation did not compromise the cytotoxicity of TRAIL on cancer cells (Figure 6c). The ability of TRAIL-conjugated Si particles to adhere to immobilized fibrin under flow was also tested. TRAIL conjugation at 0.2, 0.5, and 1 μg per mg of Si particles did not affect particle adhesion with statistical significance (Figure 6d).

Killing of CTCs in lung vasculature by TRAIL-conjugated PMDV-Si particles

To investigate the ability of PMDV-camouflaged Si particles to target CTCs in circulation, 10^5 red fluorescently labeled MDA-MB-231 cells were injected via tail vein injection into NSG mice. 30 min after injection, the mice received retro-orbital injections of 5×10^6 FITC-labeled PMDV-Si particles or uncoated Si particles. Shortly after injection, lungs were collected, immediately fixed with formaldehyde and snap frozen by liquid nitrogen for tissue sectioning. Fibrin was stained in sections for localization of cancer cell-induced thrombosis in the lung vasculature. The number of PMDV-Si particles colocalized within cancer cell/

fibrin “clusters” were quantified from 20 randomly selected clusters derived from three mouse lung images and compared the average number to that of uncoated Si particles. It was found that PMDV-Si particles were able to efficiently target cancer cell-fibrin clusters while uncoated particles were not (Figure 7a–c).

The ability of PMDV-coated Si particles to co-localize with CTCs suggested a Trojan horse strategy of delivering cancer-specific cytotoxic drugs such as TRAIL to neutralize CTCs in circulation. To test this idea, an experimental lung metastasis model was utilized by inoculating mice with MDA-MB-231 cells expressing firefly luciferase via tail vein injection. TRAIL-conjugated PMDV-Si particles (1 μg TRAIL per mg of silica) were injected via retro-orbital injection at 30, 90 and 120 min after injection of cancer cells at a particle-to-cell ratio of 50 : 1. Three control groups were included to compare the efficacy of targeted TRAIL delivery via PMDV-Si particles: TBS, PMDV-coated Si particles and soluble TRAIL (Figure 8a). Longitudinal bioluminescence imaging was performed at week 2 and 4 after the injection of cancer cells (Figure 8b and c). Quantification of bioluminescence in lungs indicated ~40 fold reduction of lung metastases in the experimental group compared to TBS and PMDV-Si particle controls. Moreover, TRAIL-conjugated PMDV-Si particles showed ~8 fold reduction compared to soluble TRAIL (Figure 8d). Following the mouse sacrifice at week 4, the lung metastases were examined histologically through H&E staining and immunohistochemistry using an anti-luciferase antibody. In vehicle control groups (TBS and PMDV-Si particle), the lungs developed metastases throughout entire lobes with severely compromised airways, whereas the soluble TRAIL treatment group showed scattered large tumor nodules. In contrast, the TRAIL-conjugated PMDV-Si treatment was associated with much smaller and fewer tumor nodules than those in the soluble TRAIL group (Figure 9a and b). The identity of tumor cells in lung lobes was further confirmed with an anti-luciferase antibody (Figure 9c).

Biodistribution and biological safety of TRAIL-conjugated PMDV-Si particles *in vivo*

To study the biodistribution of the TRAIL-conjugated PMDV-Si particles in mice, 5×10^6 TRAIL-conjugated PMDV-Si particles were injected into mice via tail vein injection. Particles were pre-labeled with Cy5. At 12 and 24 hr time points, whole body imaging was performed before euthanizing the mice. The liver, spleen, kidney, heart, lung, brain and blood samples were collected, weighed, homogenized and subjected to measurement of fluorescence intensity. It was found that by the 24 hr time point, the majority of particles accumulated in the liver and spleen (Supplemental figure 6a and b). This indicated that particles were cleared mainly from liver and spleen.

Previous studies indicated that a major side effect for TRAIL is induction of hepatocyte apoptosis associated with high dosages of TRAIL [29, 30]. Considering this factor, the liver toxicity was first tested in tumor-free NSG mice with the same dose and frequency (i.e. 0, 30, and 90 min time points) as described above. After 24 hr, livers were collected and were subjected to TUNEL staining for apoptotic cells. As with vehicle controls (TBS and PMDV-Si particles), neither soluble TRAIL nor TRAIL-conjugated PMDV-Si particles induced detectable apoptosis in liver cells. DNase I treatment of liver sections was used as a positive control for TUNEL staining (Supplemental figure 7a and b). In addition to the TUNEL

assay, no necrotic areas were found in H&E staining of liver sections from mice that received soluble TRAIL or TRAIL-conjugated PMDV-Si particles compared to those from the vehicle control group mice (TBS and PMDV-Si particles) (Supplemental figure 7c and d).

A tail bleeding test was also performed to examine whether TRAIL-conjugated PMDV-coated Si particles would interfere with blood coagulation *in vivo*. Tumor-free NSG mice receiving the same dose and frequency (i.e. 0, 30, and 90 min time points) retro-orbitally as described above were subjected to tail bleeding immediately after the last administration of particles or controls. No significant difference in bleeding time was detected in PMDV-coated Si particles or TRAIL-conjugated PMDV-coated Si particles relative to vehicle control (TBS) (Supplemental figure 7e). This suggests that the treatment will have no significant effect on coagulation.

Conclusion

In the past decades, numerous studies have identified receptor-ligand interactions between activated platelets and cancer cells, including but not limited to P selectin ligands (cancer cells)-P selectin (platelets), $\alpha_{IIb}\beta_3$ integrins (both cancer cells and platelets)-fibrinogen (in plasma), and $\alpha_2\beta_1$ integrins (both cancer cells and platelets)-collagen (extracellular matrix) [31, 32]. Inspired by these molecular interactions, nanotechnologies have sought to mimic activated platelets by conjugating antibodies or peptide sequences that recognize cancer cells [33, 34]. Nevertheless, existing platelet biomimetic strategies represent a bottom-up approach and may have certain limitations: the bottom-up approach is largely inadequate in duplicating a complex protein makeup of natural platelets on a synthetic substrate. The heterogeneity and complexity of cancer biology, however, suggest that not all cancer cells or cancer types utilize the same receptor-ligand interactions for platelet-cancer cell adhesion. Therefore, mis-targeting or off-targeting can be associated with this strategy. In addition, the cost of producing target antibodies or peptides at a clinical grade may become prohibitively expensive when these biomimetic formulations require scale up.

In contrast to the bottom-up strategy, a top-down approach that utilizes platelet membrane-derived vesicles (PMDVs) to coat synthetic particles may have several advantages: (1) Our study demonstrated that PMDVs in principle maintain a whole makeup of membrane proteins and glycans from platelet membranes that are relevant to CTC targeting. Moreover, molecules involved in self-recognition (e.g. CD47) of host cells for overcoming phagocyte-mediated phagocytosis are also displayed on PMDV-coated Si particles; (2) The facile access to sufficient human platelet-rich plasma (PRP) which is routinely collected clinically for platelet transfusions allows for scaling up of such a platform at relatively low cost.

Conventional methods seek to introduce polymeric conjugates (e.g. PEG) to avoid opsonization leading to reduced phagocytosis [35]. In contrast, it has been shown that the CD47 protein expressed by host cells mediates anti-phagocytosis through interactions with signal regulatory protein-α (SIRPα) expressed on phagocytes [36]. Therefore, a more biologically inspired approach has been developed by conjugating synthetic particles with CD47 or the minimal interacting peptide of CD47 to reduce phagocytosis and extend the

half-life of particles in blood circulation [37]. In addition to CD47, it remains unclear if host cells also utilize other proteins to antagonize the phagocyte-mediated phagocytosis. Therefore, a top-down biomimetic strategy as utilized in PMDV coating of Si particles may be of interest when other potential proteins for anti-phagocytosis remain unidentified.

Future investigations could engineer particles with a platelet-like disc shape (e.g. plateloid silica particles) for functionalization with platelet membrane. Plateloid particles without any targeting moiety have been demonstrated to exhibit more efficient tumoritropic accumulation in solid tumors by taking advantage of hydrodynamic forces and interfacial interactions with tumor-associated endothelium [38]. Nevertheless, it hasn't been studied whether such an advantage would also apply for targeting of CTCs in circulation. It is likely that disc-shaped particles coated with platelet membrane are more resistant to fluid shear stress when targeting fibrin-associated CTCs. In addition, an ultrasoft hydrogel with great deformability has been recently demonstrated to simulate the behavior of platelets to collapse at fibrin networks with optimal clotting effect [39]. Combining these two physical features (disc shape and deformability) with platelet membrane functionalization might form the basis for particles that more closely share the physical properties of platelets in the future.

Supplementary Material

Refer to Web version on PubMed Central for supplementary material.

Acknowledgments

We thank Christine M. Peterson and David E. Mooneyhan for assistance with animal experiments at the Cornell Center for Animal Resources and Education (CARE). We thank Lynn Dong for assistance in imaging IHC slides by ScanScope at the Immunopathology R&D Lab of Cornell University. This work was supported by NIH/NCI grant CA143876 (M.R.K).

References

1. Mehlen P, Puisieux A. Metastasis: a question of life or death. Nature reviews Cancer. 2006; 6(6): 449–58. [PubMed: 16723991]
2. Chambers AF, Groom AC, MacDonald IC. Dissemination and growth of cancer cells in metastatic sites. Nat Rev Cancer. 2002; 2(8):563–72. [PubMed: 12154349]
3. Dawidczyk CM, et al. State-of-the-art in design rules for drug delivery platforms: Lessons learned from FDA-approved nanomedicines. Journal of controlled release : official journal of the Controlled Release Society. 2014; 187C:133–144. [PubMed: 24874289]
4. Bertrand N, et al. Cancer nanotechnology: the impact of passive and active targeting in the era of modern cancer biology. Advanced drug delivery reviews. 2014; 66:2–25. [PubMed: 24270007]
5. Li J, et al. Nanobiotechnology for the Therapeutic Targeting of Cancer Cells in Blood. Cellular and Molecular Bioengineering. 2015:1–14.
6. Chauhan VP, Jain RK. Strategies for advancing cancer nanomedicine. Nature materials. 2013; 12(11):958–62. [PubMed: 24150413]
7. Jain RK. Normalizing Tumor Microenvironment to Treat Cancer: Bench to Bedside to Biomarkers. Journal of Clinical Oncology. 2013; 31(17):2205–U210. [PubMed: 23669226]
8. Placke T, et al. Platelet-derived MHC class I confers a pseudonormal phenotype to cancer cells that subverts the antitumor reactivity of natural killer immune cells. Cancer Res. 2012; 72(2):440–8. [PubMed: 22127925]

9. Granot Z, et al. Tumor entrained neutrophils inhibit seeding in the premetastatic lung. Cancer Cell. 2011; 20(3):300–14. [PubMed: 21907922]
10. Gul N, et al. Macrophages eliminate circulating tumor cells after monoclonal antibody therapy. The Journal of clinical investigation. 2014; 124(2):812–23. [PubMed: 24430180]
11. Aerts JG, Hegmans JP. Tumor-specific cytotoxic T cells are crucial for efficacy of immunomodulatory antibodies in patients with lung cancer. Cancer research. 2013; 73(8):2381–8. [PubMed: 23580578]
12. Palumbo JS, et al. Fibrinogen is an important determinant of the metastatic potential of circulating tumor cells. Blood. 2000; 96(10):3302–3309. [PubMed: 11071621]
13. Biggerstaff JP, et al. Soluble fibrin augments platelet/tumor cell adherence in vitro and in vivo, and enhances experimental metastasis. Clinical & Experimental Metastasis. 1999; 17(8):723–730. [PubMed: 10919717]
14. Rosenberg SA. IL-2: the first effective immunotherapy for human cancer. Journal of immunology. 2014; 192(12):5451–8.
15. Rizza P, Moretti F, Belardelli F. Recent advances on the immunomodulatory effects of IFN-alpha: implications for cancer immunotherapy and autoimmunity. Autoimmunity. 2010; 43(3):204–9. [PubMed: 20187707]
16. Hejna M, Raderer M, Zielinski CC. Inhibition of metastases by anticoagulants. Journal of the National Cancer Institute. 1999; 91(1):22–36. [PubMed: 9890167]
17. Amirkhosravi A, et al. Assessment of Anti-Metastatic Effects of Anticoagulant and Antiplatelet Agents Using Animal Models of Experimental Lung Metastasis. Anticoagulants, Antiplatelets, and Thrombolytics, Second Edition. 2010; 663:241–259.
18. Wang S. The promise of cancer therapeutics targeting the TNF-related apoptosis-inducing ligand and TRAIL receptor pathway. Oncogene. 2008; 27(48):6207–15. [PubMed: 18931688]
19. Mitchell MJ, et al. TRAIL-coated leukocytes that kill cancer cells in the circulation. Proceedings of the National Academy of Sciences of the United States of America. 2014; 111(3):930–5. [PubMed: 24395803]
20. Li J, Sharkey CC, King MR. Piperlongumine and immune cytokine TRAIL synergize to promote tumor death. Scientific reports. 2015; 5:9987. [PubMed: 25984950]
21. Zhang W, et al. A humanized single-chain antibody against beta 3 integrin inhibits pulmonary metastasis by preferentially fragmenting activated platelets in the tumor microenvironment. Blood. 2012; 120(14):2889–98. [PubMed: 22879538]
22. Bubendorf L, et al. Metastatic patterns of prostate cancer: an autopsy study of 1,589 patients. Human pathology. 2000; 31(5):578–83. [PubMed: 10836297]
23. Minn AJ, et al. Genes that mediate breast cancer metastasis to lung. Nature. 2005; 436(7050):518–524. [PubMed: 16049480]
24. Mazumder A, Rosenberg SA. Successful immunotherapy of natural killer-resistant established pulmonary melanoma metastases by the intravenous adoptive transfer of syngeneic lymphocytes activated in vitro by interleukin 2. The Journal of experimental medicine. 1984; 159(2):495–507. [PubMed: 6141211]
25. Headrick JR, et al. Surgical treatment of hepatic and pulmonary metastases from colon cancer. The Annals of thoracic surgery. 2001; 71(3):975–9. discussion 979–80. [PubMed: 11269484]
26. Labelle M, Begum S, Hynes RO. Direct Signaling between Platelets and Cancer Cells Induces an Epithelial-Mesenchymal-Like Transition and Promotes Metastasis. Cancer Cell. 2011; 20(5):576–590. [PubMed: 22094253]
27. Sobota A, et al. Binding of IgG-opsonized particles to Fc gamma R is an active stage of phagocytosis that involves receptor clustering and phosphorylation. Journal of immunology. 2005; 175(7):4450–4457.
28. Martinez-Sales V, et al. Unstimulated and thrombin-stimulated platelets binding to immobilized fibrinogen and fibrin on polystyrene supports. Haemostasis. 1995; 25(4):158–65. [PubMed: 7557654]
29. Volkmann X, et al. Increased hepatotoxicity of tumor necrosis factor-related apoptosis-inducing ligand in diseased human liver. Hepatology. 2007; 46(5):1498–508. [PubMed: 17705261]

30. Zheng SJ, et al. Critical roles of TRAIL in hepatic cell death and hepatic inflammation. The Journal of clinical investigation. 2004; 113(1):58–64. [PubMed: 14702109]
31. Erpenbeck L, Schon MP. Deadly allies: the fatal interplay between platelets and metastasizing cancer cells. Blood. 2010; 115(17):3427–3436. [PubMed: 20194899]
32. Gay LJ, Felding-Habermann B. Contribution of platelets to tumour metastasis. Nature Reviews Cancer. 2011; 11(2):123–134. [PubMed: 21258396]
33. Modery-Pawlowski CL, Gupta AS. Heteromultivalent ligand-decoration for actively targeted nanomedicine. Biomaterials. 2014; 35(9):2568–79. [PubMed: 24411677]
34. Modery-Pawlowski CL, et al. A platelet-mimetic paradigm for metastasis-targeted nanomedicine platforms. Biomacromolecules. 2013; 14(3):910–9. [PubMed: 23360320]
35. Immordino ML, Dosio F, Cattel L. Stealth liposomes: review of the basic science, rationale, and clinical applications, existing and potential. International Journal of Nanomedicine. 2006; 1(3): 297–315. [PubMed: 17717971]
36. Oldenborg PA, et al. Role of CD47 as a marker of self on red blood cells. Science. 2000; 288(5473):2051. [PubMed: 10856220]
37. Rodriguez PL, et al. Minimal “Self” Peptides That Inhibit Phagocytic Clearance and Enhance Delivery of Nanoparticles. Science. 2013; 339(6122):971–975. [PubMed: 23430657]
38. van de Ven AL, et al. Rapid tumoritropic accumulation of systemically injected plateloid particles and their biodistribution. Journal of Controlled Release. 2012; 158(1):148–155. [PubMed: 22062689]
39. Brown AC, et al. Ultrasoft microgels displaying emergent platelet-like behaviours. Nature materials. 2014; 13(12):1108–14. [PubMed: 25194701]

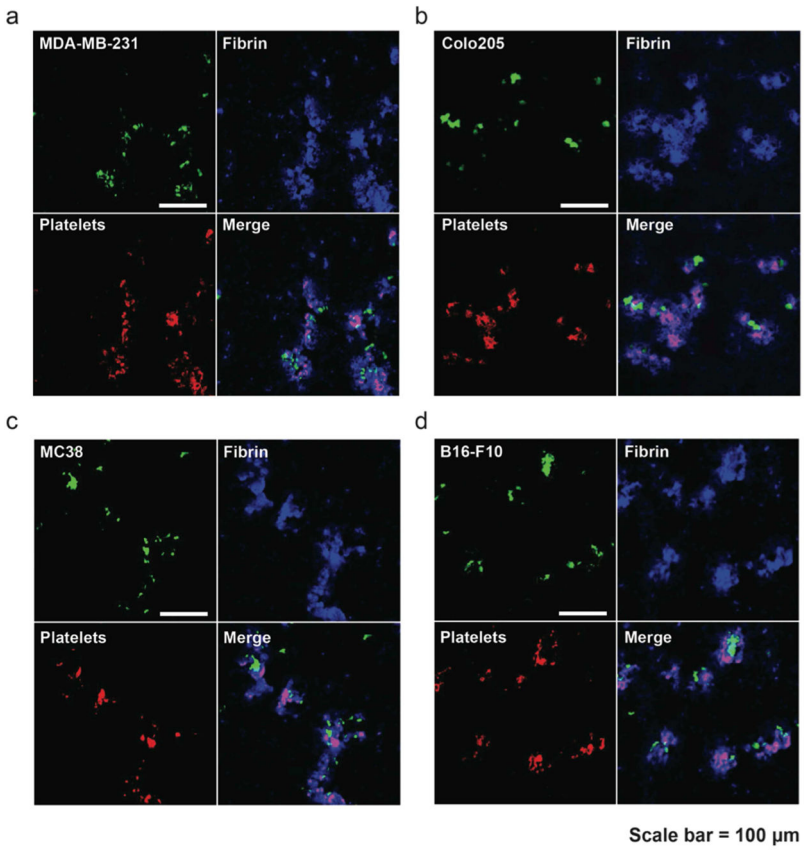

Figure 1. Co-localization of cancer cells/fibrin/platelets in lung vasculature

Immunofluorescence staining of platelets ($CD41^+$) and fibrin in lung sections with circulating CTCs. Calcein-AM-labeled human cancer cells (a) MDA-MB-231 and (b) COLO 205 were intravenously injected into NSG immunocompromised mice. After 30 min, lung sections were prepared for immunofluorescence staining of fibrin and $CD41^+$, a marker for platelets. In a syngeneic metastasis model, C57BL/6-derived cancer cells (c) MC38 and (d) B16-F10 were injected into C57BL/6 followed by staining of fibrin and platelets in lung sections.

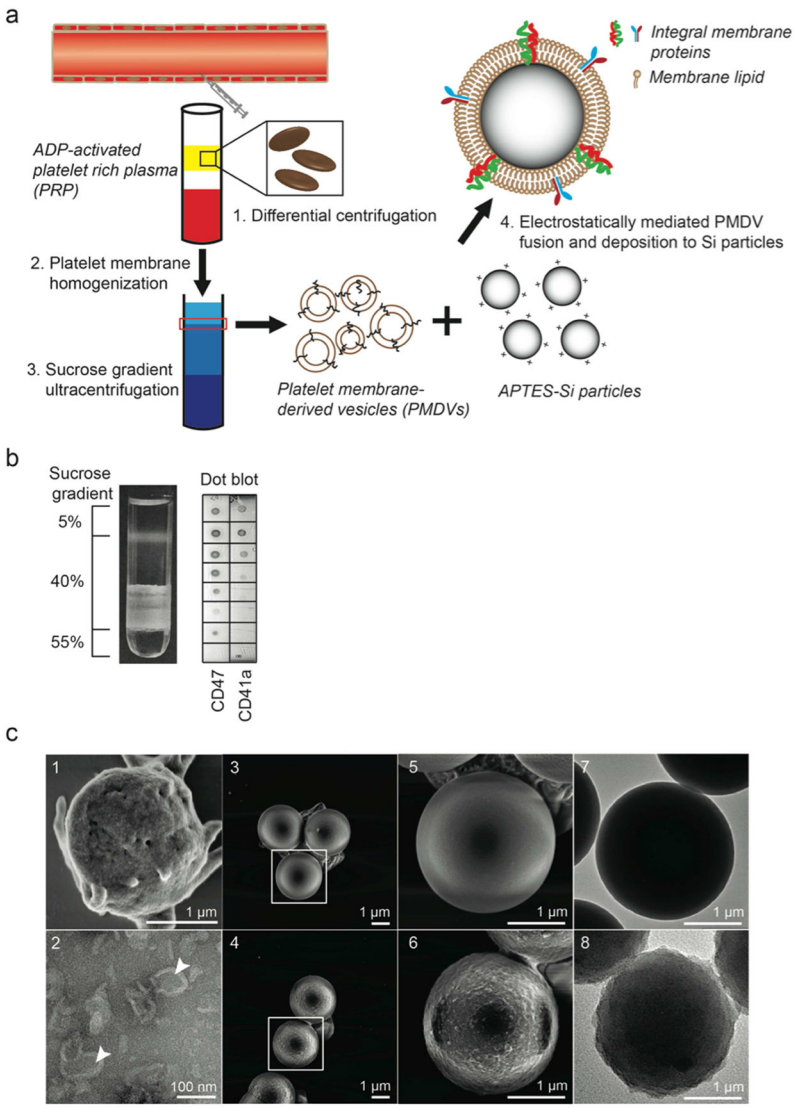

Figure 2. Functionalization and characterization of PMDV-coated Si particles

(a) Schematic of preparing platelet membrane-coated Si particles. (b) Detection of membrane protein-associated lipid layer in discontinuous sucrose gradient solution by dot blot assay. Lipid fractions were identified as translucent layers in between two sucrose concentrations. (c) SEM and TEM characterization. SEM images: (1) Activated platelets, (3, 5) APTES-Si particles, (4, 6) PMDV-coated Si particles. TEM images: (2) PMDVs, (7) APTES-Si particles, (8) PMDV-coated Si particles. Arrow head identifies the hollow structure of PMDVs.

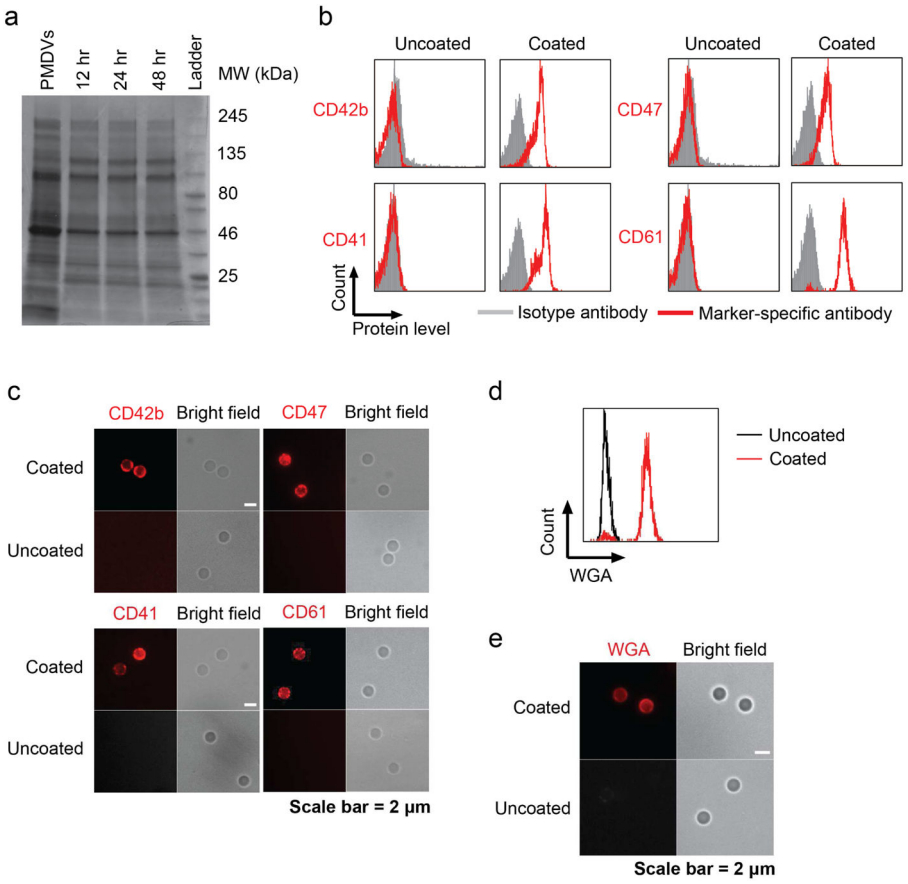

Figure 3. Presence of glycoproteins and glycans on PMDV-coated Si particles

(a) Stability of PMDV-coated Si particles. Membrane proteins were stripped after incubation of coated particles in TBS at 37 °C for 12, 24, and 48 hr. Afterwards, proteins were separated and stained by Commassie blue in SDS-PAGE. PMDVs were loaded as a positive control. (b) Detection of platelet membrane glycoproteins CD42b, CD47, CD41, and CD61 by flow cytometry. (c) Immunofluorescence staining of CD42b, CD47, CD41, and CD61 in PMDV-coated or uncoated Si particles. Far-red and bright field images were presented. (d) Detection of sialic acid and N-acetylglucosaminyl glycans on PMDV-coated Si particles. Sialic acid and N-acetylglucosaminyl residues were identified by fluorescently labeled wheat germ agglutinin (WGA) in both flow cytometry and immunofluorescence staining.

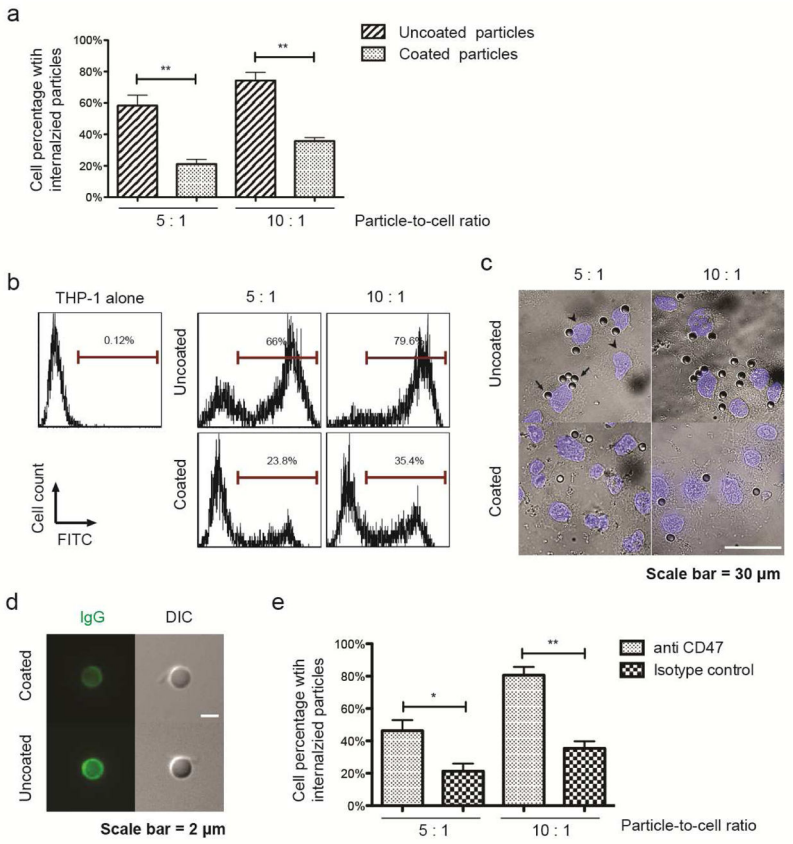

Figure 4. Reduction of particle phagocytosis via PMDV coating

(a) Internalization of uncoated and PMDV-coated Si particles in phagocytic cells. FITC-labeled Si particles were incubated with PMA-differentiated THP-1 at particle-to-cell ratios of 5:1 and 10:1. Cells with internalized particles were quantified by flow cytometry after removal of surface bound particles by trypsin. Results are presented as the mean ± SEM, n=3; **, $p<0.01$. (b) Representative flow cytometry histograms of phagocytic THP-1 cells with internalized Si particles. (c) Representative images of phagocytic THP-1 cells with internalized Si particles. After removing surface bound Si particles by trypsin, cells were cytospun onto glass slides. Nuclei were stained by DAPI (blue). Arrows: Si particles; arrowheads: nuclei. (d) Differential opsonization of human IgG to the surface of uncoated and PMDV-coated Si particles. After 30 min incubation with human serum, washed particles were stained with FITC-labeled anti-hIgG Fc. Particles were imaged through green fluorescent and DIC channels. (e) CD47 was partially responsible for reduced phagocytosis of PMDV-coated Si particles. FITC-labeled PMDV-coated Si particles were preincubated with anti-CD47 blocking antibody and subsequently added to PMA-differentiated THP-1 cells. Cells with internalized particles were quantified by flow cytometry. Results are presented as the mean ± SEM; n=3; *, $p<0.05$; **, $p<0.01$.

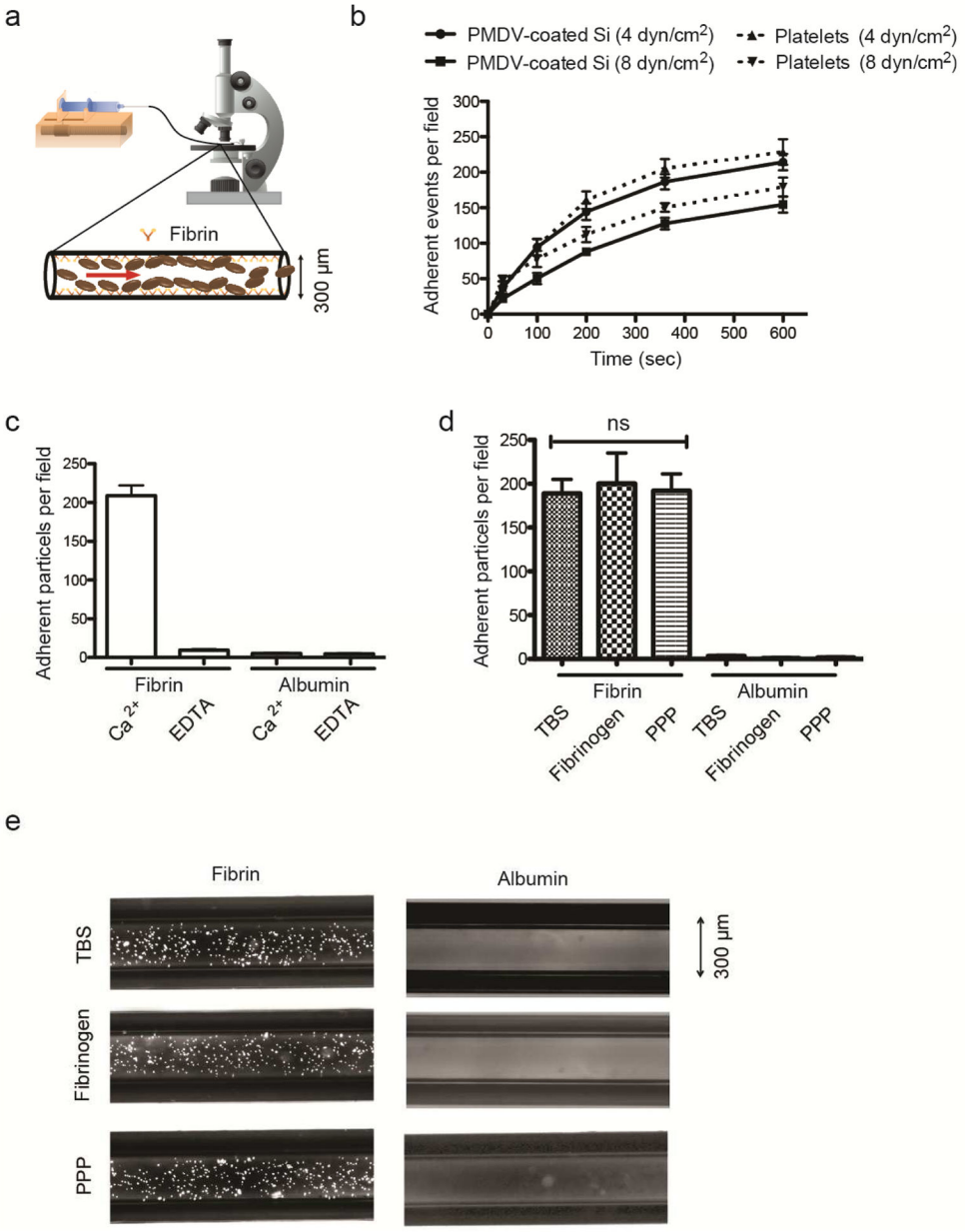

Figure 5. Adhesion of PMDV-coated Si particles to immobilized fibrin under flow

(a) Schematics of a microtube with the inner surface coated with fibrins to simulate blood clotting. 10^6/ml PMDV-coated Si particles were perfused through microtubes at 4 dyn/cm^2 via a controlled syringe pump. (b) Adhesion of coated particles and activated platelets to a fibrin-functionalized surface under flow. (c) Comparison of adherent particles in Ca^{2+}- or EDTA-containing buffer under flow. For negative control, albumin was coated on the surface in the absence of fibrin. (d) Comparison of particle adhesion to fibrin-coated microtubes under flow in tris-buffered saline (TBS), TBS containing 2 mg/ml soluble fibrinogen or platelet poor plasma (PPP). TBS buffer was supplemented with Ca^{2+}. Results are presented as the mean ± SEM; ns indicates no significant difference. (e) Representative

fluorescent images of adherent particles in fibrin-coated microtubes were taken after removing unbound particles via TBS washing.

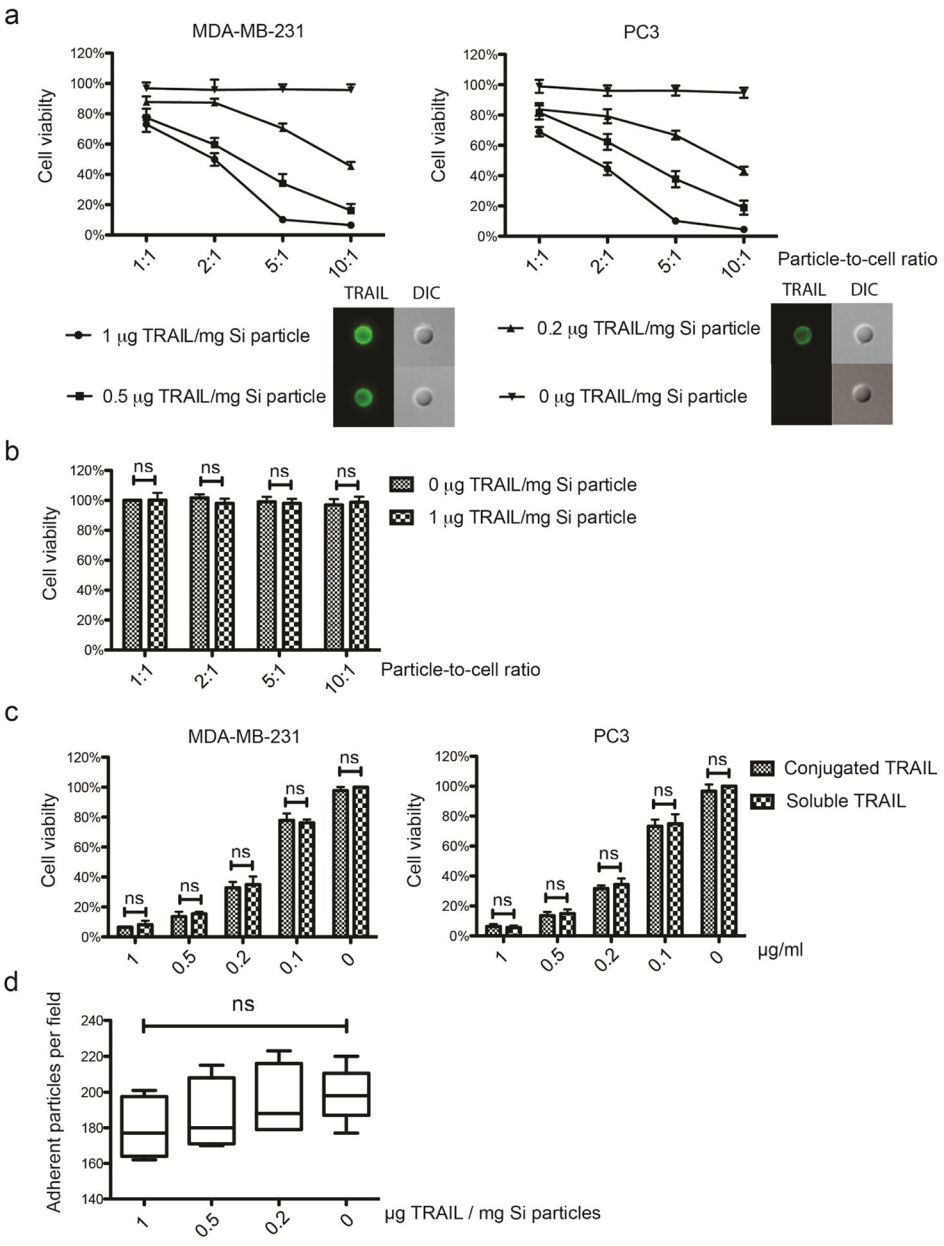

Figure 6. Conjugation of TRAIL to PDMV-coated Si particles induced apoptosis in cancer cells

The density of TRAIL on the surface of PDMV-coated particles was varied at 0, 0.2, 0.5, and 1 μg TRAIL/mg Si particles. (a) TRAIL was immunostained by FITC-anti human TRAIL. PDMV-coated particles with TRAIL conjugation of varied density were incubated with breast cancer cells MDA-MB-231 and prostate cancer cells PC3 at particle-to-cell ratios of 1:1, 2:1, 5:1, and 10:1 for 24 hr. Cell viability was measured by MTT assay. (b) TRAIL conjugation on PMDV-coated Si particles was nontoxic to endothelial cells. PMDV Si particles at a conjugation density of 0 or 1 μg TRAIL/mg Si particles were incubated with HUVECs with different particle-to-cell ratios. Cell viability in each treatment group was normalized to the treatment with 0 μg TRAIL/mg Si particles at 1:1 particle-to-cell ratio. (c)

Comparing efficacy of soluble TRAIL versus TRAIL immobilized to PDMV-coated Si particles in inhibition of cancer cell proliferation. PMDV-coated Si particles (1 μg TRAIL/mg silica coating density) were incubated with cancer cells at different particle-to-cell ratios and compared to soluble TRAIL at a concentration matched to respective particle-to-cell ratios. (d) TRAIL conjugation did not interfere with the ability of PDMA-coated Si particles to adhere to a fibrin-immobilized surface under flow. All results are presented as the mean ± SEM, n=3; ns indicates no significant difference.

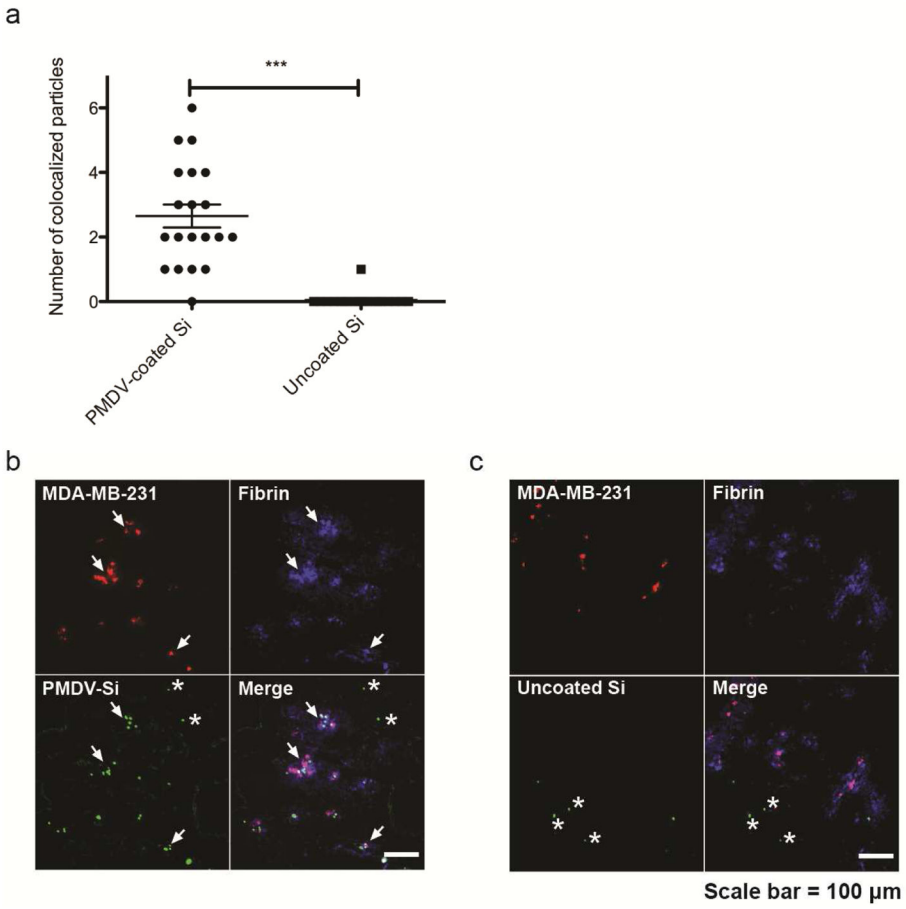

Figure 7. Targeting of PMDV-coated Si particles to CTC/fibrin micro-thrombi in lungs

(a) Quantification of PDMV-Si particles versus uncoated particles colocalized within cancer cell/fibrin "clusters". One cluster is defined by having at least one cancer cell or a few cancer cells that are physically close to each other. Results are presented as the mean ± SEM, n=20, ***, $p<0.001$). Representative colocalization images of (b) PMDV-coated Si particles and (c) uncoated Si particles. Stars mark off-target particles. Arrows indicate clusters.

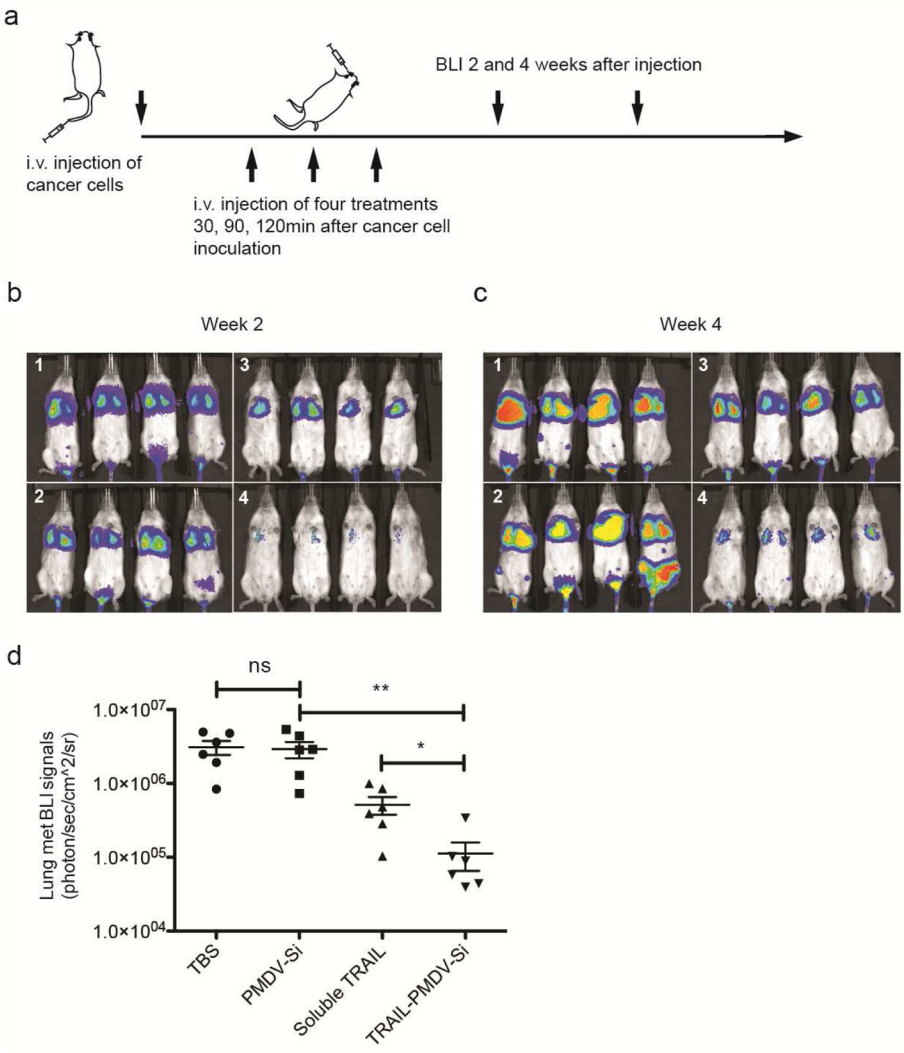

Figure 8. Reduction of lung metastasis by TRAIL-conjugated PMDV-Si particles

(a) Schematic of experimental protocol for the lung metastasis model and therapeutic treatment. BLI at 2 weeks (b) and 4 weeks (c) after cancer cell injection. Four different treatment groups were applied: 1. TBS; 2. PMDV-Si particles; 3. Soluble TRAIL; 4. TRAIL-conjugated PMDV-Si particles. (d) Quantification of lung metastasis in different treatment groups at week 4. All results are presented as the mean ± SEM, n=6; *, $p<0.05$; **, $p<0.01$; ns indicates no significant difference.

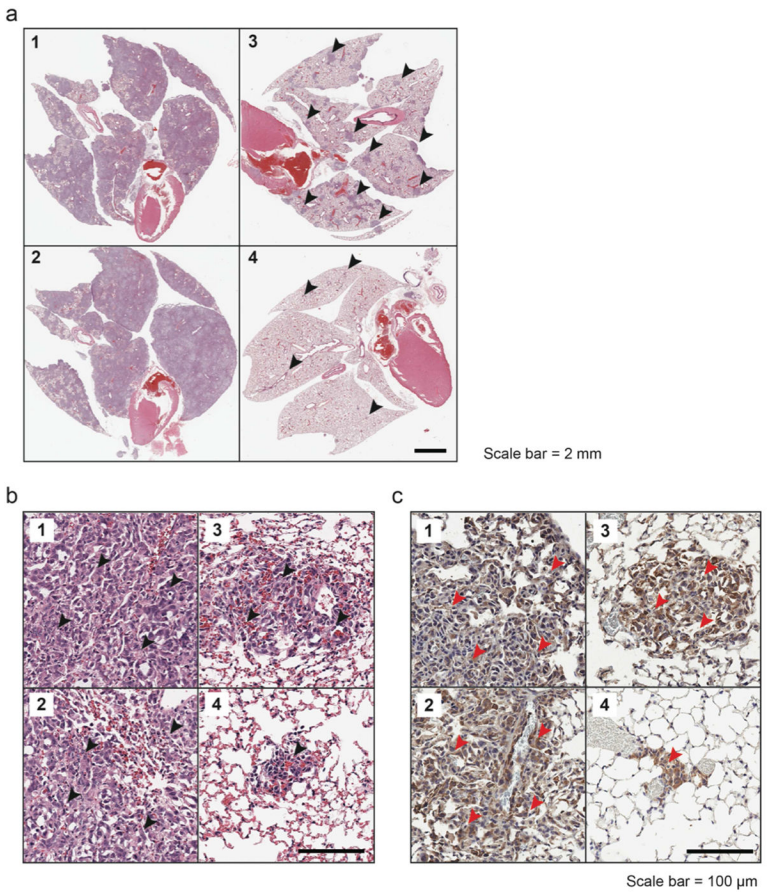

Figure 9. Histological examination of lung metastasis in response to TRAIL-conjugated PMDV-Si particles

Lungs were collected at week 4 from the four different treatment groups: 1. TBS; 2. PMDV-Si particles; 3. Soluble TRAIL; 4. TRAIL-conjugated PMDV-Si particles. Images were taken at (a) low and (b) high magnifications, respectively. Arrowheads indicate tumor areas or nodules. (c) Immunohistochemistry staining of lung sections for luciferase-expressing cancer cells using anti-luciferase antibody.

Table 1

Particle characterization

	Size (nm)	Zeta potential (mV)
Platelets	2320 ± 185	−9.8 ± 3.1
Platelet-derived vesicles	106 ± 12	−10.5 ± 2.4
Si particles	2008 ± 34	−20.8 ± 3.2
APTES Si particles	2085 ± 48	25.5 ± 4.6
Membrane-coated Si particles	2293 ± 92	−10.1 ± 1.9

Table 2

Top platelet membrane integral proteins identified by LC-MS

Name	Functions	Receptors
THBS1	Platelet adhesion	Fibrinogen, fibronectin, laminin, and collagen
Integrin α 2b (CD41)	$\alpha_{IIb}\beta_3$ complex, platelet adhesion and aggregation	Fibrinogen, fibronectin, vWF
Integrin β, β_3 (CD61)	$\alpha_{IIb}\beta_3$ complex, platelet adhesion and aggregation	Fibrinogen, fibronectin, vWF
GP Ib α (CD42b)	GPIb-V-IX complex, platelet adhesion	vWF
GP Ib β (CD42c)	GPIb-V-IX complex, platelet adhesion	vWF
GP IX	GPIb-V-IX complex, platelet adhesion	vWF
GP V	GPIb-V-IX complex, platelet adhesion	vWF
GP VI	Initial platelet adhesion	Collagen
MHC-1	Host recognition, self compatibility	CD8 receptor
CD47	Anti-phagocytosis	Signal regulatory protein-α (SIRPα)
P-selectin	Platelet adhesion	PSGL-1 (decorated with sLe^x)